

# A simple formulation of the CH<sub>2</sub>O photolysis quantum yields

E.-P. Röth<sup>1</sup> and D. H. Ehhalt<sup>2</sup>

[1]{Institute for Energy and Climate Research (IEK-7: Stratosphere), Research Center Jülich, Germany}

[2]{Institute for Energy and Climate Research (IEK-8: Troposphere), Research Center Jülich, Germany}

Correspondence to: E.-P. Röth (e.p.roeth@fz-juelich.de)

## Abstract

New expressions for the wavelength-dependent photolysis quantum yields of CH<sub>2</sub>O,  $\Phi_j$ , are presented. They are based on combinations of functions of the type  $A_i/(1+\exp[-(1/\lambda-1/\lambda_{0i})/b_i])$ . The parameters  $A_i$ ,  $b_i$ , and  $\lambda_{0i}$  which have a physical meaning are obtained by fits to the measured data of the  $\Phi_j$  available from the literature. The altitude dependence of the photolysis frequencies resulting from the new quantum yield expressions are compared to those derived from the  $\Phi_j$  recommended by JPL and IUPAC.

## 1. Introduction

Formaldehyde, CH<sub>2</sub>O, is an important trace gas in the atmosphere. It is formed as an intermediate in the oxidation of methane and non-methane hydrocarbons, and destroyed by the reaction with OH and by photolysis in the near ultraviolet. The photolysis involves several channels. Following the excitation (R1), CH<sub>2</sub>O\* can decay into purely molecular products (R2), or into products that in the atmosphere lead to the eventual formation of hydroperoxy radicals, HO<sub>2</sub>, (R3, R4). The quenching reaction R5 and fluorescence R6 can influence the quantum yields of the product channels.



As it turns out the molecular channel, R2, provides the by far largest source of molecular hydrogen, H<sub>2</sub>, in the atmosphere (Ehhalt and Rohrer, 2009). The radical channels, R3 and R4, that generate HO<sub>2</sub> radicals, enhance local photochemistry. Finally each destruction of a CH<sub>2</sub>O

1 molecule – including that by OH – eventually results in a carbon monoxide molecule, CO. As  
2 a consequence, CH<sub>2</sub>O is also an important source of CO in the atmosphere.

3 Recognizing the importance for atmospheric chemistry the quantum yields of the CH<sub>2</sub>O  
4 photolysis were measured early on and by various authors (see Sander et al., 2011, Atkinson  
5 et al., 2006, and the internet version IUPAC (2013) for summaries).

6 The quantum yield  $\Phi_{\text{mol}}$  of the molecular branch R2 was usually measured by monitoring the  
7 H<sub>2</sub> production while scavenging the H atoms to prevent their contribution to the H<sub>2</sub>  
8 production (e.g., Moortgat et al., 1978, Horowitz and Calvert, 1978). The formation of the  
9 molecular products via the reaction path of a roaming H-atom [see e.g., Bowman and Shepler,  
10 2011 and Christoffel and Bowman, 2009] was not known then and is not included explicitly  
11 in our list of reactions but it is included in reaction R2, and its quantum yield is part of the  
12 measured  $\Phi_{\text{mol}}$ .

13 Reactions R3 and R4 form the radical channel with the combined quantum yield  $\Phi_{\text{rad}}$  which  
14 in some cases was investigated directly by measuring the products, H and CHO (e.g., Smith et  
15 al., 2002, Gorrotxategi et al., 2008, Tatum Ernest et al., 2012).

16 The fluorescence quantum yield (R6) was measured by Miller and Lee, 1978, in the  
17 wavelength range 290 to 360 nm. Its maximum at 353 nm is less than 3.5 % and it is less than  
18 1% at the other wavelengths considered. It will, therefore, be neglected here. We know of no  
19 measurements below 290 nm.

20 The total quantum yield  $\Phi_{\text{tot}}$ , i.e. the fraction of the decay of excited formaldehyde, CH<sub>2</sub>O\*,  
21 into products other than its ground state, was derived from the CO production. By definition  
22  $\Phi_{\text{tot}}$  is the sum of the quantum yields of the molecular and the radical channel:

$$23 \quad \Phi_{\text{tot}} = \Phi_{\text{mol}} + \Phi_{\text{rad}} \quad (1)$$

24 The measured wavelength dependences of the quantum yields are usually given in tabular  
25 form (see e.g., Atkinson et al., 2006, IUPAC, 2013). For  $\Phi_{\text{rad}}$  also a fit by a fourth order  
26 polynomial (see Sander et al., 2011) exists. To provide a more handy tool for atmospheric  
27 modeling we propose to use sums of energy dependent functions of the type

$$28 \quad \frac{A}{1 + \exp\left[\frac{-(1/\lambda - 1/\lambda_0)}{b}\right]} \quad (2)$$

29 to fit  $\Phi_{\text{mol}}$  and  $\Phi_{\text{rad}}$ . These functions are well-suited to map smooth transitions. They allow to  
30 include pressure and temperature dependences. And the resulting parameters are few and have  
31 a physical meaning: in particular  $1/\lambda_0$  corresponds to the threshold energy of the respective  
32 reaction; b describes the width of the transitions. Moreover, the formalism should also provide  
33 a useful template for the formulation of the analogous  $\Phi_i$  for the isotopologues of

1 formaldehyde. In particular we hope to eventually construct expressions of the quantum yields  
2 for CHDO for which – apart from the threshold energies and a few isotope fractionation  
3 factors- no direct measurements exist.

4 Our analysis of the quantum yields will be based on the data filed by JPL (Sander et al., 2011)  
5 and IUPAC (2006) omitting all measurements whose wavelength dependencies deviate  
6 strongly from the forms recommended by JPL or IUPAC (e.g., McQuigg and Calvert, Clark et  
7 al., Tang et al. for  $\Phi_{\text{rad}}$ ). Likewise, if measured data appear in several publications by the same  
8 authors, only the latest data were considered. Not all data are independent of each other, as  
9 some measurements (Smith et al., 2002, Pope et al., 2005, Tatum Ernest et al., 2012) are  
10 relative and normalized to absolute quantum yields (DeMore et al., 1997, Sander et al., 2011).  
11 This influences the uncertainty range of the parameters  $A_i$  whose  $1\sigma$  errors might be  
12 somewhat larger than indicated in the respective equations.

13 First, in Sections 2 to 4, we will fit the measured wavelength dependences of the various  $\Phi$   
14 separately and compare them to those reported in the literature. In a second step, after having  
15 convinced ourselves that the parameters from the separate fits that should correspond to each  
16 other are indeed similar in value, we attempt a simultaneous fit of all  $\Phi$  in Chapter 5.

17

## 18 **2. The quantum yield of the radical channel**

19 Most publications on the formaldehyde photolysis deal with the radical channel R3 - notably:  
20 Horowitz and Calvert (1978), Moortgat et al. (1983), Smith et al. (2002), Gorrotxategi et al.  
21 (2008), and Tatum Ernest et al. (2012). Nearly all of these measurements were made at room  
22 temperature, and experiments and theory indicate that there is no pressure dependence of  $\Phi_{\text{rad}}$ .  
23 We, therefore, assume all these data to be comparable and their variance attributable to  
24 experimental error. Thus all these data are combined in Figure 1. Smith et al. (2002) attributed  
25 some of the variance in their data to a line structure in  $\Phi_{\text{rad}}$ . The possibility of a line structure  
26 is corroborated by the data of Tatum Ernest et al. (2012), which show a strong feature in  $\Phi_{\text{rad}}$   
27 at 321 nm. For comparison, the data of Tatum Ernest et al. are also shown in Figure 1, but  
28 they are not used for the fit.

29 To fit the experimentally observed wavelength dependence of  $\Phi_{\text{rad}}$  we use a combination of  
30 two functions of the type mentioned above, one for the decay of  $\Phi_{\text{rad}}$  to longer wavelengths at  
31 about 328 nm, the other for the decay towards shorter wavelengths at 277 nm. To obtain the  
32 fit parameters and their errors a simplex algorithm (Nelder and Mead, 1965) is used in  
33 combination with a bootstrapping method with 2000 arbitrary removals of 20 % of the data.  
34 The result is given by Eq. (3), with  $\lambda$  in nm:

$$\Phi_{rad} = \frac{0.72 \pm 0.01}{1 + \exp\left(\frac{-\left(\frac{1}{\lambda} - \frac{1}{328.0 \pm 0.6}\right)}{(5.2 \pm 0.6) \cdot 10^{-5}}\right)} - \frac{0.38 \pm 0.03}{1 + \exp\left(\frac{-\left(\frac{1}{\lambda} - \frac{1}{278.4 \pm 0.8}\right)}{(4.7 \pm 1.1) \cdot 10^{-5}}\right)} \quad (3)$$

Equation 3 is also shown in Fig.1.

Eq. (3) holds primarily for room temperature. The respective parameters will be labelled by the subscripts l,s. They stand for the short and long wavelength region. The index m, introduced below in Section 5 stands for the intermediate wavelength. The  $\lambda_0$  mark the inflection points in the decays:  $\lambda_{0,l} = 328.0$  nm;  $\lambda_{0,s} = 278.4$  nm. The corresponding b define the wavelength interval within which the decrease takes place. Owing to the scatter in the measured  $\Phi_{rad}$  data all these parameters exhibit an uncertainty range. The estimated 1  $\sigma$  errors of the parameters are also entered in Equation 3 . We note that  $\lambda_{0,l}$  closely corresponds to the dissociation energy of the H-CHO bond namely  $30328.5$  cm<sup>-1</sup> or 329.7 nm (Terentis et al., 1998) and that  $\lambda_{0,s}$  approximately corresponds to the heat of reaction of R4 namely 423 kJ/mol or 283 nm (Sander et al., 2011).

Moortgat et al. (1983) have also measured the wavelength dependence of  $\Phi_{rad}$  at 220 K. Given the experimental variance in those admittedly sparse data, Eq. (3) also fits the measured  $\Phi_{rad}$  at 220 K quite well (not shown here). Thus, as far as the experimental data on  $\Phi_{rad}$  are concerned, Eq. (3) covers the temperature range of 220 K to 300 K relevant for atmospheric modeling and there is no immediate need to introduce a temperature dependence. On the other hand, theoretical considerations suggest the inclusion of the internal energy of the CH<sub>2</sub>O molecule, and this can be easily done. Following Troe (2007) one can add a term 3kT (appropriately scaled) to  $1/\lambda$  in the left hand term of Eq. (3). In Section 6 we will investigate the impact of this T dependence (see Eq. 12) on the altitude profile of the respective photolysis frequency. In principle, another weak T dependence can arise through the parameter b. That dependence could be easily accommodated by replacing b by  $(b_0 + b_1T)$  should future  $\Phi_{rad}$  measurements provide enough information to warrant such a step. The present formulation of Eq. (3) with constant parameters b - i.e. b independent of  $\lambda$  - forces the decrease to be nearly symmetrical around the respective  $\lambda_0$ . This is not necessarily realistic. Again, if future measurements or theoretical considerations should prove the need, an asymmetry could be easily accommodated by allowing b to depend on  $\lambda$ .

Finally, we note, that a line structure could be superimposed on Eq. (3) without difficulty. For the moment we refrain from doing so for two reasons: 1) As Tatum Ernest et al. (2012) already indicated even the strong feature in  $\Phi_{rad}$  at 321 nm produces only a small change in the photolysis frequencies in the atmosphere. In fact, superposition of this feature on Equation

1 3 would increase  $j_{\text{mol}}$  by less than 2 % at all altitudes and decrease  $j_{\text{rad}}$  by less than 4%,  
2 because it coincides with a small value in the absorption coefficient of  $\text{CH}_2\text{O}$ . Thus the error  
3 possibly introduced by the neglect of the line structure is comparatively small (see discussion  
4 below). 2) The measurements of  $\Phi_{\text{rad}}$  by Smith et al. (2002), and Gorrotxategi et al. (2008)  
5 contain data points close to 321 nm which fall right on the average  $\Phi_{\text{rad}}$  given by Eq. (3).  
6 They were made with sufficient resolution to resolve the feature at 321 nm and are therefore  
7 somewhat at variance with the finding of Tatum Ernest et al. (2012).  
8 Fig. 1 also contains the recommended wavelength dependences of  $\Phi_{\text{rad}}$  given in the  
9 evaluations by JPL (Sander et al., 2011), IUPAC (2006), and IUPAC (2013). The reason for  
10 the inclusion of IUPAC (2006) is that these data, which were first published in 2002 and  
11 remained in the internet until 2012, had many users in the past and possibly still have users at  
12 present. Further included is the theory-based dependence derived by Troe (2007); it covers  
13 only the restricted wavelength range from 310 to 350 nm. As a quantitative measure of the  
14 quality of these fits we here add the coefficient of determination  $cd$ . In the present case this is  
15 identical to the correlation coefficient between fitted and measured data. These correlation  
16 coefficients are:  $cd = 0.821$  (IUPAC, 2006);  $cd = 0.840$  (Troe, 2007);  $cd = 0.898$  (JPL, 2011);  
17  $cd = 0.876$  (IUPAC, 2013), and  $cd = 0.905$  (this work); that is the quality of these various fits  
18 does not differ drastically.

19

### 20 **3. The total quantum yield**

21 There are more direct measurements for  $\Phi_{\text{tot}}$  and its dependence on  $\lambda$  than for  $\Phi_{\text{mol}}$ . To obtain  
22 higher accuracy we, therefore, first obtain a fit for  $\Phi_{\text{tot}}(\lambda)$  and then use Eq. (1), i.e.  $\Phi_{\text{mol}} = \Phi_{\text{tot}}$   
23  $- \Phi_{\text{rad}}$  for a fit of  $\Phi_{\text{mol}}(\lambda)$ . That fit is later compared to the measured dependence of  $\Phi_{\text{mol}}$  on  $\lambda$ .  
24 The available measurements of  $\Phi_{\text{tot}}(\lambda)$  at 300 K temperature and 1013 hPa pressure are  
25 reproduced in Figure 2. The values of  $\Phi_{\text{tot}}$  at 355 nm and 353 nm were obtained by  
26 interpolating the respective Stern-Volmer plots given by Moortgat et al. (1979, 1983) to the  
27 pressure of 1 atm. The  $\Phi_{\text{tot}}$  values at  $\lambda < 340$  nm are pressure independent. The measured  
28  $\Phi_{\text{tot}}(\lambda)$  exhibits three regions: a plateau between 290 and 330 nm, a steep decrease to zero at  
29 longer wavelengths, and a weak decrease to  $\Phi_{\text{tot}} \sim 0.8$  at shorter wavelengths. The average  
30 measured  $\Phi_{\text{tot}}$  in the plateau is  $1.06 \pm 0.09$  – not significantly different from 1 – the maximum  
31 possible value. Therefore, in the fit we fixed this value to unity. The separation of the two  
32 decreases by a plateau with  $\Phi_{\text{tot}} = 1$  also means that it is possible to fit these two regions of  
33 decrease separately and independently of each other.

1 The measurements in Figure 1 indicate that  $\Phi_{\text{rad}}$  vanishes at  $\lambda > 340$  nm; at those wavelengths  
 2  $\Phi_{\text{tot}}$  becomes identical to  $\Phi_{\text{mol}}$ . Moreover, tunneling processes extend the photolysis of  $\text{CH}_2\text{O}$   
 3 to  $\text{H}_2$  and  $\text{CO}$  well beyond the threshold energy of about 350 nm (Troe, 2007). In this energy  
 4 regime the rate of decay into the molecular channel decreases to values where collisional  
 5 quenching of the excited formaldehyde molecule (R5) begins to compete. Consequently,  $\Phi_{\text{mol}}$   
 6 and  $\Phi_{\text{tot}}$  become pressure dependent. Based on theoretical modeling and comparison with the  
 7 data of Moortgat et al. (1978, 1983), Troe (2007) proposed a Stern-Volmer formulation for  
 8  $\Phi_{\text{mol}}$  for  $\lambda > 340$  nm:

$$9 \quad \Phi_{\text{mol}} = \frac{1}{1 + 1.4 \exp(c(\lambda - \lambda_0)) (M/M_0)} \quad (4)$$

10 with  $\lambda_0 = 349$  nm;  $c = 0.225 \text{ nm}^{-1}$  for  $\lambda > \lambda_0$  and  $c = 0.205 \text{ nm}^{-1}$  for  $\lambda < \lambda_0$  and  $M$  the number  
 11 density of the bath gas.  $M_0 = 2.46 \times 10^{19} \text{ cm}^{-3}$ , the number density at 1013 hPa pressure and  
 12 300 K temperature. Troe (2007) also pointed out that on theoretical grounds the temperature  
 13 dependence of  $\Phi_{\text{mol}}$  should be small compared to the experimental uncertainties and thus  
 14 negligible at this stage. This is somewhat at variance to the measurements by Moortgat et al.  
 15 (1983) which seem to indicate such a dependency, albeit with large uncertainties.

16 Since  $\Phi_{\text{tot}}$  equals  $\Phi_{\text{mol}}$  for  $\lambda > 340$  nm where nearly all of the change in  $\Phi_{\text{tot}}$  with wavelength  
 17 is located, and since Eq. (4) approaches unity for  $\lambda < 330$  nm, Eq. (4) should also provide a  
 18 good approximation for  $\Phi_{\text{tot}}(\lambda)$ . In fact we could use it with its current parameters as our  
 19 intended fit (see Figure 2).

20 However, we prefer to formulate our fit in terms of energy, i.e.  $1/\lambda$ . Moreover, a direct fit to  
 21 the data in Figure 2 will merge the pre-exponential factor in Eq. (4) with  $\lambda_0$ . So, instead of  
 22 using Eq. (4) we will fit Eq. (5) to the data at  $\lambda > 310$  nm in Figure 2:

$$23 \quad \Phi_{\text{tot}} = \frac{1}{1 + \exp\left(\frac{-\left(1/\lambda - 1/\lambda_{0,l}\right)}{b_l}\right)} \cdot (M/M_0) \quad (5)$$

24 Our fit yields the parameters  $\lambda_{0,l}$  and  $b_l$  of Eq.(6). In this case  $\lambda_{0,l}$  has a somewhat different  
 25 meaning than before. Here,  $\lambda_{0,l}$  not only depends on the threshold energy of the reaction  
 26 involved, but also on the quenching efficiency with which energy is drained from the excited  
 27  $\text{CH}_2\text{O}$  molecule. But as before,  $\lambda_{0,l}$  represents the inflection point in the decrease of  $\Phi$ , at least  
 28 for  $M = M_0$ .

29 The fit for the short wave decrease adds the second term in Eq. (6) for  $\Phi_{\text{tot}}$ . The equation for  
 30  $\Phi_{\text{tot}}(\lambda)$  over the full wavelength range therefore is:

$$\Phi_{tot} = \frac{1}{1 + \exp\left(\frac{-(1/\lambda^{-1}/347.1 \pm 0.7)}{(5.7 \pm 0.8) \times 10^{-5}}\right)} \left(\frac{M}{M_0}\right) - \frac{0.20 \pm 0.01}{1 + \exp\left(\frac{-(1/\lambda^{-1}/284.3 \pm 0.9)}{(3.5 \pm 1.4) \times 10^{-5}}\right)} \quad (6)$$

2 with  $\lambda$  given in nm.

3 We have not been able to find a ready explanation for the experimentally observed weak  
4 decrease of  $\Phi_{tot}$  at shorter wavelengths in the literature. We note, however, that  $\lambda_{0,s}=284.3$   
5 corresponds closely to the heat of reaction for R4 (see Section 2).

6 Following the arguments by Troe (2007) we assume the temperature dependence of  $\Phi_{tot}(\lambda)$  to  
7 be negligible. But here again, our fitting functions could readily be modified to include a T  
8 dependence.

9  $\Phi_{tot}(\lambda)$  from Eq. (6) is also shown in Figure 2. It compares favorably to the measured data of  
10  $\Phi_{tot}$ . For additional comparison Figure 2 also contains the recommended wavelength  
11 dependences of  $\Phi_{tot}$  given in the evaluations by JPL (Sander et al., 2011), IUPAC (2013), and  
12 IUPAC (2006). Further included is the dependence derived from Troe's (2007)  $\Phi_{mol}$ ; it covers  
13 only the restricted wavelength range from 310 to 370 nm. Just as Eq. (6), the  $\Phi_{tot}(\lambda)$  from JPL  
14 and that based on Troe (2007) agree well with the measurements. An exception are the  
15 recommended values from IUPAC (2006) which clearly deviate from the measurements in the  
16 range  $330 \text{ nm} < \lambda < 350 \text{ nm}$ . The consequence of this deviation on the coefficient of  
17 determination is relatively small:  $cd = 0.913$ , whereas the others are: JPL,  $cd = 0.959$ ; Troe,  
18  $cd = 0.944$ ; present,  $cd = 0.956$ . In IUPAC (2013) this deviation is removed; the  
19 corresponding  $cd$  is 0.924.

20

#### 21 **4. The quantum yield of the molecular channel**

22 Since  $\Phi_{mol}$  is given by  $\Phi_{tot} - \Phi_{rad}$ , it could be simply obtained from the difference of Eqs. (6)  
23 and (3). On the other hand,  $\Phi_{mol}$  can be obtained by a direct fit to the measured data. This  
24 requires a combination of only three functions of the Eq. (2) type and the fit results in:

$$\Phi_{mol} = \frac{1}{1 + \exp\left(\frac{-(1/\lambda^{-1}/345.2 \pm 0.8)}{(6.2 \pm 1.7) \times 10^{-5}}\right)} \left(\frac{M}{M_0}\right) - \frac{0.75 \pm 0.03}{1 + \exp\left(\frac{-(1/\lambda^{-1}/325.3 \pm 0.6)}{(3.9 \pm 0.5) \times 10^{-5}}\right)} + \frac{0.24 \pm 0.05}{1 + \exp\left(\frac{-(1/\lambda^{-1}/274.2 \pm 3.3)}{(2.3 \pm 2.1) \cdot 10^{-5}}\right)} \quad (7)$$

27 Eq. (7) makes the implicit assumption that the short wave decreases in  $\Phi_{tot}$  and  $\Phi_{rad}$  have the  
28 same  $\lambda_{0,s}$  and  $b_s$ . The estimated  $1\sigma$  errors of the fit parameters are entered in Eq. (7).

1 In Figure 3,  $\Phi_{\text{mol}}(\lambda)$  from Eq. (7) is compared to the measured data on  $\Phi_{\text{mol}}(\lambda)$ . The latter  
2 consist of direct measurements of  $\Phi_{\text{mol}}$  by Moortgat et al. (1979; 1983), and data based on  
3 measured  $\Phi_{\text{tot}}$  and  $\Phi_{\text{rad}}$  by Horowitz and Calvert (1978). The agreement of Eq. (7) with the  
4 measurements is quite reasonable. For further comparison Figure 3 also includes the  
5 recommendations by JPL (Sander et al., 2011), IUPAC (2013), and IUPAC (2006) as well as  
6 a fit based on  $\Phi_{\text{tot}}$  and  $\Phi_{\text{rad}}$  derived from Troe (2007). The respective coefficients of  
7 determination are:  $cd = 0.822$  (IUPAC, 2006);  $cd = 0.838$  (Troe, 2007);  $cd = 0.947$   
8 (JPL;2011)  $cd = 0.843$  (IUPAC, 2013);  $cd = 0.958$  (this work).

9

## 10 **5. Simultaneous fit of $\Phi_{\text{rad}}$ , $\Phi_{\text{mol}}$ , and $\Phi_{\text{tot}}$**

11 A comparison of the parameters and their errors obtained from the individual fits of the  
12 various  $\Phi$  suggests that the  $\lambda_{0,s}$ ,  $\lambda_{0,m}$ ,  $\lambda_{0,l}$  and  $b_s$ ,  $b_m$ ,  $b_l$  in a given fit equation do not differ  
13 significantly from the corresponding parameters in the others. We, therefore, felt justified to  
14 attempt a simultaneous fit of all  $\Phi$ . In this attempt we assume that the corresponding  $\lambda_0$  and  $b$   
15 parameters in the various equations for  $\Phi$  are indeed identical. We further assume that  $\Phi_{\text{tot}}$   
16 reaches a maximum value of 1 and that Eq. (1) holds. With these assumptions the total  
17 number of fit parameters for all three  $\Phi$  together reduces to 9. The simultaneous calculation of  
18 the 9 unknown parameters results in the equations for the  $\Phi_i$  listed in Table 1, their estimated  
19  $1\sigma$  errors are also entered in the equations.

20 The functions of Table 1 differ somewhat, but hardly significantly from those given by Eqs.  
21 (3), (6) and (7) considering the experimental uncertainties. The coefficients of determination  
22 are comparable to those from the individual fits:  $c=0.904$  for  $\Phi_{\text{rad}}$ ,  $0.951$  for  $\Phi_{\text{tot}}$ , and  $0.934$  for  
23  $\Phi_{\text{mol}}$ . Because of their simplicity Eqs. (8)- (10) represent our preferred formulation of the  
24  $\text{CH}_2\text{O}$  quantum yields and will be used in the discussion below.

25

## 26 **6. Discussion**

27 In the foregoing sections we presented new formulations of  $\Phi_{\text{tot}}$ ,  $\Phi_{\text{rad}}$ , and  $\Phi_{\text{mol}}$  for  $\text{CH}_2\text{O}$ . The  
28 presentation also made it clear that there is room for improvements. One concerns the  
29 temperature dependence of  $\Phi$ . Given the experimental uncertainties we have refrained from  
30 providing T dependences for the  $\Phi$ 's . But there are temperature dependences in the literature,  
31 which could be incorporated in our formulation (Atkinson et al., 2006; Troe, 2007; Sander et  
32 al., 2011). Below we will incorporate such a temperature dependence in  $\Phi_{\text{rad}}$  to test the



1 sensitivity of the corresponding photolysis frequencies of CH<sub>2</sub>O to the vertical temperature  
2 profile.

3 In addition, the question of line structure in  $\Phi_{\text{rad}}$  needs eventually to be resolved.

4 Of major interest to the atmospheric chemists is the impact of this new formulation of  $\Phi$  on  
5 the atmospheric photolysis frequencies of CH<sub>2</sub>O. That photolysis frequency  $j$  is given by:

$$6 \quad j = \int_0^{\infty} \Phi(\lambda) \sigma(\lambda) F_{\lambda}(\lambda) d\lambda \quad (11)$$

7 i.e. it also depends on the absorption cross-section,  $\sigma(\lambda)$ , of CH<sub>2</sub>O, and the local actinic  
8 photon flux density  $F_{\lambda}(\lambda)$ . For our calculations of  $j$  we will use the absorption spectrum  
9 measured by Gratien et al. (2007). It is, by the way, also slightly temperature dependent; the  
10 respective function can be found in Röth et al. (1997). Its effect on the  $j_i$  is quite small – e.g.  
11 less than 0.3 % for  $j_{\text{rad}}$  – and included in the calculations. The atmospheric actinic photon flux  
12 density consists of down-welling and up-welling contributions, and depends of course on the  
13 solar zenith angle and altitude. It was calculated by the radiative transfer program ART (Röth,  
14 2002) using the extraterrestrial solar flux from WMO (1985). All three factors under the  
15 integral strongly vary with wavelength,  $\lambda$ . (To various degrees they also vary with altitude.)  
16 As an example Figure 4 shows  $\sigma(\lambda)$ ,  $F_{\lambda}(\lambda)$ , and  $\Phi_{\text{mol}}(\lambda)$ , together with the wavelength  
17 dependent integrand of Eq.(11) at 30 km altitude and 33° solar zenith angle. We particularly  
18 notice the sharp cutoff in  $F_{\lambda}(\lambda)$  around  $\lambda = 320$  nm caused by the absorption of solar UV in  
19 the ozone layer at lower wavelengths. This means that below 30 km altitude the exact form of  
20 the  $\Phi_i$  at  $\lambda < 300$  nm has little influence on the various photolysis frequencies. Figure 4  
21 further indicates how much the long-wave decrease of  $\Phi_{\text{mol}}$  is shifted towards longer  
22 wavelengths at the air density at 30 km altitude. In fact, this shift is so large that the long-  
23 wave cutoff of the integrand in Eq. (11) is no longer determined by  $\Phi_{\text{mol}}$ , as it is at low  
24 altitudes, but rather by the absorption spectrum of CH<sub>2</sub>O. Hence, at altitudes above 30 km the  
25 exact form of the decrease in  $\Phi_{\text{mol}}$  and  $\Phi_{\text{tot}}$  at the longer wavelengths has no influence on the  
26 respective photolysis frequencies. The curve for  $\sigma \cdot \Phi \cdot F_{\lambda}$  in Fig.4 nicely illustrates why the line  
27 structure observed by Tatum Ernest et al. (2012) at 321 nm has so little impact on  $j_{\text{mol}}$ : It  
28 would increase the quite small feature at 321 nm in that product by only a factor of 1.5.  
29 Given the  $\Phi_i$  from the Eqs. (8) to (10) in Table 1,  $\sigma(\lambda)$  from Gratien et al. (2007) along with  
30 vertical temperature and density profiles of the U.S. standard atmosphere (NOAA, 1976) we  
31 can calculate the vertical profiles of the photolysis rates. The calculations were made with 1  
32 nm spectral resolution and are shown in Figure 5. The shaded areas mark the  $1\sigma$  error bounds  
33 of the  $j_i$  profiles based on the errors of the fitting parameters for  $\Phi_i$  given in Section 5. As to

1 be expected, all  $j_i$  increase with altitude. In the case of  $j_{rad}$  that increase is essentially due to  
 2 the vertical change in  $F_\lambda(\lambda)$ , since our  $\Phi_{rad}$  is neither temperature nor pressure dependent and  
 3 thus independent of altitude, and the slight temperature dependence of  $\sigma(\lambda)$  makes a minor  
 4 contribution only.  $j_{tot}$  and  $j_{mol}$ , however, are significantly modified by the density dependence  
 5 in  $\Phi_{mol}$ .

6 In Figure 5 we also demonstrate the impact of a possible temperature dependence in  $\Phi_{rad}$ . The  
 7 temperature dependence is introduced by adding the term  $(300-T)(3k/hc)$  in the appropriate  
 8 dimensional units to  $1/\lambda$  in the first term of Eq. (3) (see Troe, 2007, and Section 2.).

$$9 \quad \Phi_{rad} = \frac{0.74}{1 + \exp\left(\frac{-(1/\lambda + (300-T)(3k/hc) - 1/327.4)}{5.4 \cdot 10^{-5}}\right)} - \frac{0.40}{1 + \exp\left(\frac{-(1/\lambda - 1/279.0)}{5.2 \cdot 10^{-5}}\right)} \quad (12)$$

10  
 11 This means that only the long-wave decay in  $\Phi_{rad}$  is considered to be temperature dependent.  
 12 Here  $k$  is the Boltzmann constant,  $h$  the Planck constant, and  $c$  the speed of light. As Figure 5  
 13 shows, a temperature dependence of this size clearly has a significant impact on  $j_{rad}$  and by  
 14 virtue of  $\Phi_{mol} = \Phi_{tot} - \Phi_{rad}$  also on  $j_{mol}$ . The effect is largest at around 15 km, the height of the  
 15 temperature minimum, and about -9% for  $j_{rad}$ , respectively ca. +6% for  $j_{mol}$ . The temperature  
 16 at 15 km is 220 K, i.e. the temperature shifts in  $j_{rad}$  and  $j_{mol}$  correspond to a temperature  
 17 difference of 80 K. Apparently a correct formulation of the T-dependence of  $\Phi_{rad}$  could lead  
 18 to a significant change in the predicted vertical profiles of  $j_{rad}$  and  $j_{mol}$ .

19  $j_{tot}$  remains unaffected by the proposed temperature dependency. In fact, even assuming a  
 20 temperature dependence of the kind above for the long-wave decay of  $\Phi_{tot}$  would have  
 21 comparatively little impact on the  $j_{tot}$  profile. It would be masked by the air density  
 22 dependence of  $\Phi_{tot}$ . Just as at lower densities, the exact form of the long-wave decay in  $\Phi_{tot}$   
 23 no longer influences  $j_{tot}$ , so can its temperature dependence no longer influence  $j_{tot}$ .

24 Finally, in Figure 6, we compare the photolysis frequencies based on this work's quantum  
 25 yields to those calculated with the quantum yields recommended by IUPAC (2006), IUPAC  
 26 (2013), and JPL (Sander et al., 2011). The JPL recommendation includes an explicit  
 27 temperature dependence for  $\Phi_{rad}$ . In addition both, JPL and IUPAC (2006) treat the density  
 28 dependence of  $\Phi_{mol}$  in terms of atmospheric pressure, which introduces a further temperature  
 29 dependence. Both temperature effects are included in the calculation of the respective  $j_i$   
 30 profiles. The comparison demonstrates that even at present – without a representation of the  
 31 temperature dependence - our  $\Phi_i$  provide vertical profiles of the photolysis frequency which  
 32 agree well with those based on  $\Phi_i$  from the JPL recommendation - for all  $j_i$  and both solar

1 zenith angles considered. The comparison with the data from Atkinson et al. (2006) is less  
2 favorable, especially for  $j_{\text{mol}}$ . This reflects the differences between  $\Phi_{\text{mol}}(\lambda)$  given here and  
3 that recommended by JPL on the one hand to that recommended by Atkinson et al. (2006) on  
4 the other, which were already apparent in Figures 2 and 3. The new quantum yields  
5 recommended by IUPAC in 2013 give photolysis rates which lie slightly below our values for  
6  $j_{\text{mol}}$ , just outside the error bounds.

7 Although the derived  $j_i$  profiles as well as the fits to the measured  $\Phi_i$  (Figures 1 to 3) based on  
8 the JPL recommendation and on the present work appear reasonably equivalent, we feel our  
9 formalism to be advantageous. Since it consistently formulates the wavelength dependence of  
10  $\Phi_i$  in terms of  $1/\lambda$ , its fitting parameters are in units of energy, and represent, or are close to,  
11 molecular parameters, notably threshold energies, which are often available and can serve as  
12 guides. Moreover, the formulation in units of energy makes it easy to introduce temperature  
13 dependences should future measurements or theoretical considerations demand it. For the  
14 same reasons our formalism should provide a useful template for the formulation of the  $\Phi_i$  for  
15 the isotopologues of formaldehyde and likewise for the photolysis quantum yields of many  
16 other molecules.

17

## 18 **Acknowledgement**

19

20 The article processing charges for this open-access publication have been covered by a  
21 Research Centre of the Helmholtz Association.

22

## 23 **References**

24 Atkinson, R., Baulch, D. L., Cox, R. A., Crowley, J. N., Hampson, R. F., Hynes, R. G.,

25 Jenkin, M. E., Rossi, M. F., and Troe, J.: Evaluated kinetic and photochemical data for  
26 atmospheric chemistry: Volume II – gas phase reactions of organic species, *Atmos. Chem.*

27 *Phys.*, 6, 3625 – 4055, 2006

28 Bowman, J. M. and Shepler, B. C.: Roaming Radicals, *Ann. Rev. Phys. Chem.*, 62, 531 – 553,  
29 2011

30 Christoffel, K. M. and Bowman, J. M.: Three Reaction Pathways in the  $\text{H} + \text{HCO} \rightarrow \text{H}_2 + \text{CO}$   
31 Reaction, *J. Phys. Chem. A*, 113, 4138 – 4144, 2009

32 Clark, J. H., Moore, C. B., and Nogar, N. S.: The photochemistry of formaldehyde: Absolute  
33 quantum yields, radical reactions, and NO reactions, *J. Chem. Phys.*, 68, 1264 - 1271, 1978

1 DeMore, W. B., Sander, S. P., Howard, C. J., Ravishankara, A. R., Golden, D. M., Kolb, C.  
2 E., Hampson, R. F., Kurylo, M. J., Molina, M. J.: NASA panel for data evaluation, chemical  
3 kinetics and photochemical data evaluation for use in stratospheric modeling, JPL Publication  
4 97-4, 1997

5 Gorrotxategi Carbajo, P., Smith, S. C., Holloway, A.-L., Smith, C. A., Pope, F. D., Shallcross,  
6 D. E., and Orr-Ewing, A. J.: Ultraviolet photolysis of HCHO: Absolute HCO quantum yields  
7 by direct detection of the HCO Radical photoproduct, *J. Phys. Chem. A*, 112, 12437 – 12448,  
8 2008

9 Gratien, A., Nilsson, E., Doussin, J.-F., Johnson, M. S., Nielsen, C. J., Stenstrom, Y., and  
10 Picquet-Varrault, B.: UV and IR absorption cross-sections of HCHO, HCDO, and DCDO, *J.*  
11 *Phys. Chem. A*, 111, 11506 - 11513, 2007

12 Horowitz, A. and Calvert, J. G.: Wavelength dependence of the quantum efficiencies of the  
13 primary processes in formaldehyde photolysis at 25°C. *Int. J. Chem. Kinetics*, 10, 805 – 819,  
14 1978

15 IUPAC (2006) : see Atkinson et al. (2006)

16 IUPAC (2013): IUPAC Task Group on Atmospheric Chemical Kinetic Data Evaluation –  
17 Data Sheet P1, <http://iupac.pole-ether.fr>, (last access: 16 January 2015) 2013

18 McQuigg, R. D. and Calvert, J. G.: The photodecomposition of CH<sub>2</sub>O, CD<sub>2</sub>O, CHDO, and  
19 CH<sub>2</sub>O-CD<sub>2</sub>O mixtures at Xenon flash lamp intensities, *J. Am. Chem. Soc.*, 91, 1590 – 1599,  
20 1969

21 Miller, R. G. and Lee, E. K. C.: Single vibronic level photochemistry of formaldehydes in the  
22 A<sup>1</sup>A<sub>2</sub> state: Radiative and non radiative processes in H<sub>2</sub>CO, HDCO, and D<sub>2</sub>O, *J. Chem. Phys.*,  
23 68, 4448 – 4464, 1978

24 Moortgat, G. K., Slemr, F., Seiler, W., and Warneck, P.: Photolysis of formaldehyde: Relative  
25 quantum yields of H<sub>2</sub> and CO in the wavelength range 270 -360 nm, *Chem. Phys. Letters*, 54,  
26 444 – 447, 1978

27 Moortgat, G. K. and Warneck, P.: CO and H<sub>2</sub> quantum yields in the photodecomposition of  
28 formaldehyde in air, *J. Chem. Phys.*, 70, 3639 – 3651, 1979

29 Moortgat, G. K., Seiler, W., and Warneck, P.: Photodissociation of HCHO in air: CO and H<sub>2</sub>  
30 quantum yields at 220 K and 300 K, *J. Chem. Phys.*, 78, 1185 – 1190, 1983

31 Nelder, J. A. and Mead, R.: A simplex method for function minimization, *Computer Journal*,  
32 7, 308 -313, 1965

33 NOAA; U.S. Standard Atmosphere, NOAA-S/T76-1562, Washington D.C.,1976

1 Röth, E.-P.: Description of the anisotropic radiation transfer model ART to determine  
2 photodissociation coefficients, Ber. Forschungszentrum Jülich, Jül-3960, Jülich,2002  
3 Röth, E.-P., Ruhnke, R., Moortgat, G., Meller, R., and Schneider, W.: UV/VIS absorption  
4 cross sections and quantum yields for use in photochemistry and atmospheric modeling. Part  
5 2: Organic substances, Ber. Forschungszentrum Jülich, Jül-3341, Jülich,1997  
6 Sander, S. P., Friedl, R.R., Abbatt, J. P. D., Barker, J. R., Burkholder, J. B., Golden, D. M.,  
7 Kolb, C. E., Kurylo, M. J., Moortgat, G. K., Wine, P. H., Huie, R. E., and Orkin, V. L.:  
8 Chemical kinetics and photochemical data for use in atmospheric studies. Evaluation number  
9 17, JPL-Publication 10-6, Pasadena,2011  
10 Smith, G. D., Molina, L. T., and Molina, M. J.: Measurement of radical quantum yields from  
11 formaldehyde photolysis between 269 and 339 nm, J. Phys. Chem. A, 106, 1233 – 1240, 2002  
12 Tang, K. Y., Fairchild, P. W., and Lee, E. K. C.: Laser-induced photodecomposition of  
13 formaldehyde ( $A^1A_2$ ) from its single vibronic levels. Determination of the quantum yield of H  
14 atom by  $HNO^*$  ( $A^1A''$ ) chemiluminescence, J. Phys. Chem., 83, 569 – 573, 1979  
15 Tatum Ernest, C., Bauer, D., and Hynes, A. J.: Radical Quantum Yields from Formaldehyde  
16 Photolysis in the  $30\,300 - 32\,890\text{ cm}^{-1}$  (304 – 329 nm) Spectral Region: Detection of Radical  
17 Products Using Pulsed Laser Photolysis – Pulsed Laser Induced Fluorescence, J. Phys. Chem.  
18 A, 116, 6983 – 6995, 2012  
19 Terentis, A. C., Waugh, S. E., Metha, G. F., and Kable, S. H.: HCO ( $N, K_a, K_c, J$ ) distributions  
20 from near-threshold photolysis of  $H_2CO$  ( $J, K_a, K_c$ ), J. Chem. Phys. 108, 3187 – 3198, 1998  
21 Troe, J.: Analysis of quantum yields for the photolysis of formaldehyde at  $\lambda > 310\text{ nm}$ , J.  
22 Phys. Chem. A, 111, 3868 – 3874, 2007  
23 WMO: Atmospheric Ozone 1985, Vol. 1, WNO Report 16, Genf,1985  
24

1

2 **Table 1:** Recommended quantum yield functions for use in atmospheric chemistry models  
 3 (wavelength  $\lambda$  in nm).

4

$$\Phi_{rad} = \frac{0.74 \pm 0.01}{1 + \exp\left(\frac{-\left(\frac{1}{\lambda} - \frac{1}{327.4 \pm 0.5}\right)}{(5.4 \pm 0.5) \cdot 10^{-5}}\right)} - \frac{0.40 \pm 0.04}{1 + \exp\left(\frac{-\left(\frac{1}{\lambda} - \frac{1}{279.0 \pm 1.3}\right)}{(5.2 \pm 2.4) \cdot 10^{-5}}\right)} \quad (8)$$

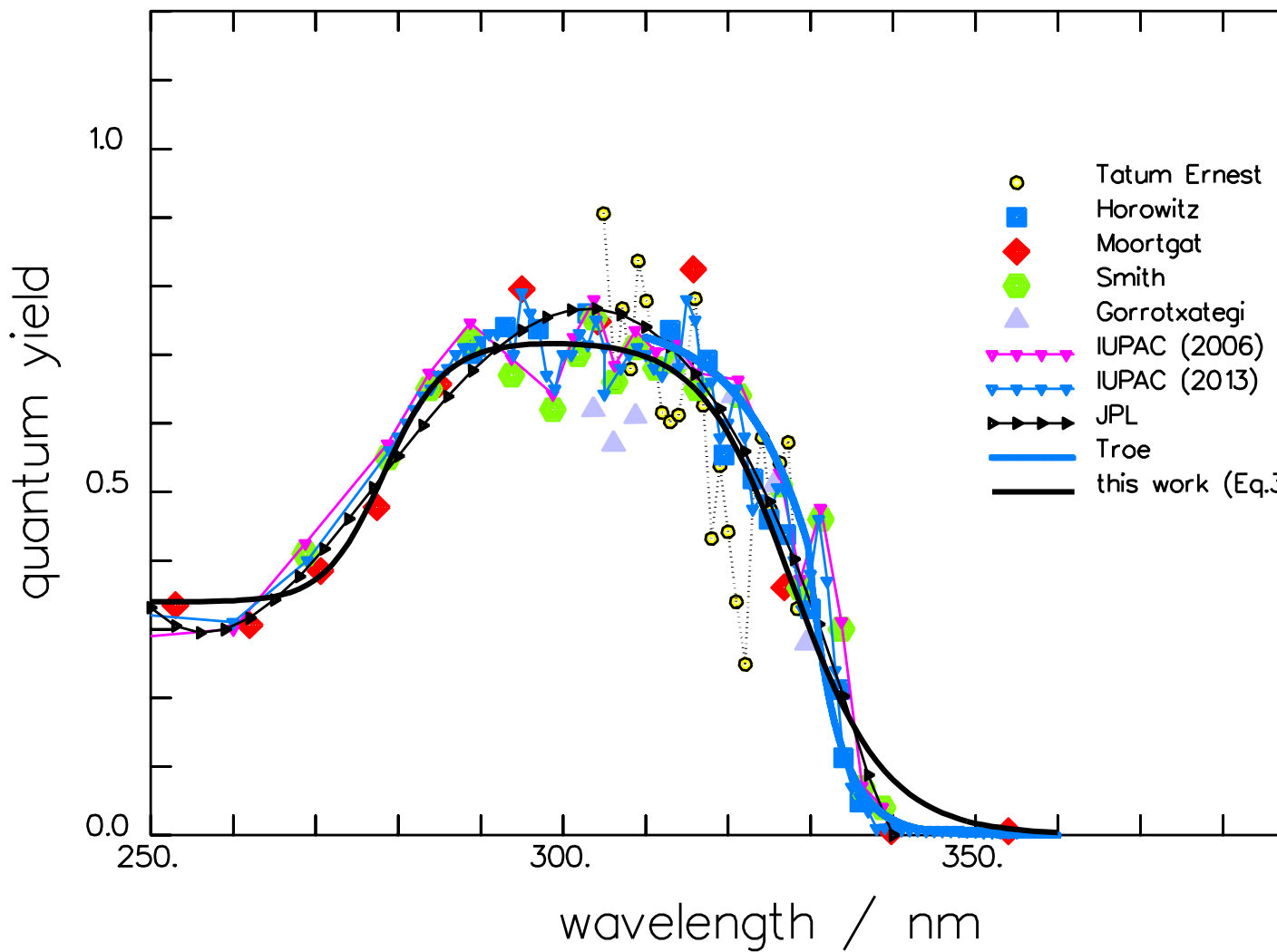
$$\Phi_{tot} = \frac{1}{1 + \exp\left(\frac{-\left(\frac{1}{\lambda} - \frac{1}{346.9 \pm 0.5}\right)}{(5.4 \pm 0.3) \times 10^{-5}}\right)} \left(\frac{M}{M_0}\right) - \frac{0.22 \pm 0.02}{1 + \exp\left(\frac{-\left(\frac{1}{\lambda} - \frac{1}{279.0 \pm 1.3}\right)}{(5.2 \pm 2.4) \times 10^{-5}}\right)} \quad (9)$$

$$\Phi_{mol} = \frac{1}{1 + \exp\left(\frac{-\left(\frac{1}{\lambda} - \frac{1}{346.9 \pm 0.5}\right)}{(5.4 \pm 0.3) \times 10^{-5}}\right)} \left(\frac{M}{M_0}\right) - \frac{0.74 \pm 0.01}{1 + \exp\left(\frac{-\left(\frac{1}{\lambda} - \frac{1}{327.4 \pm 0.5}\right)}{(5.4 \pm 0.5) \cdot 10^{-5}}\right)} + \frac{0.18 \pm 0.02}{1 + \exp\left(\frac{-\left(\frac{1}{\lambda} - \frac{1}{279.0 \pm 1.3}\right)}{(5.2 \pm 2.4) \cdot 10^{-5}}\right)} \quad (10)$$

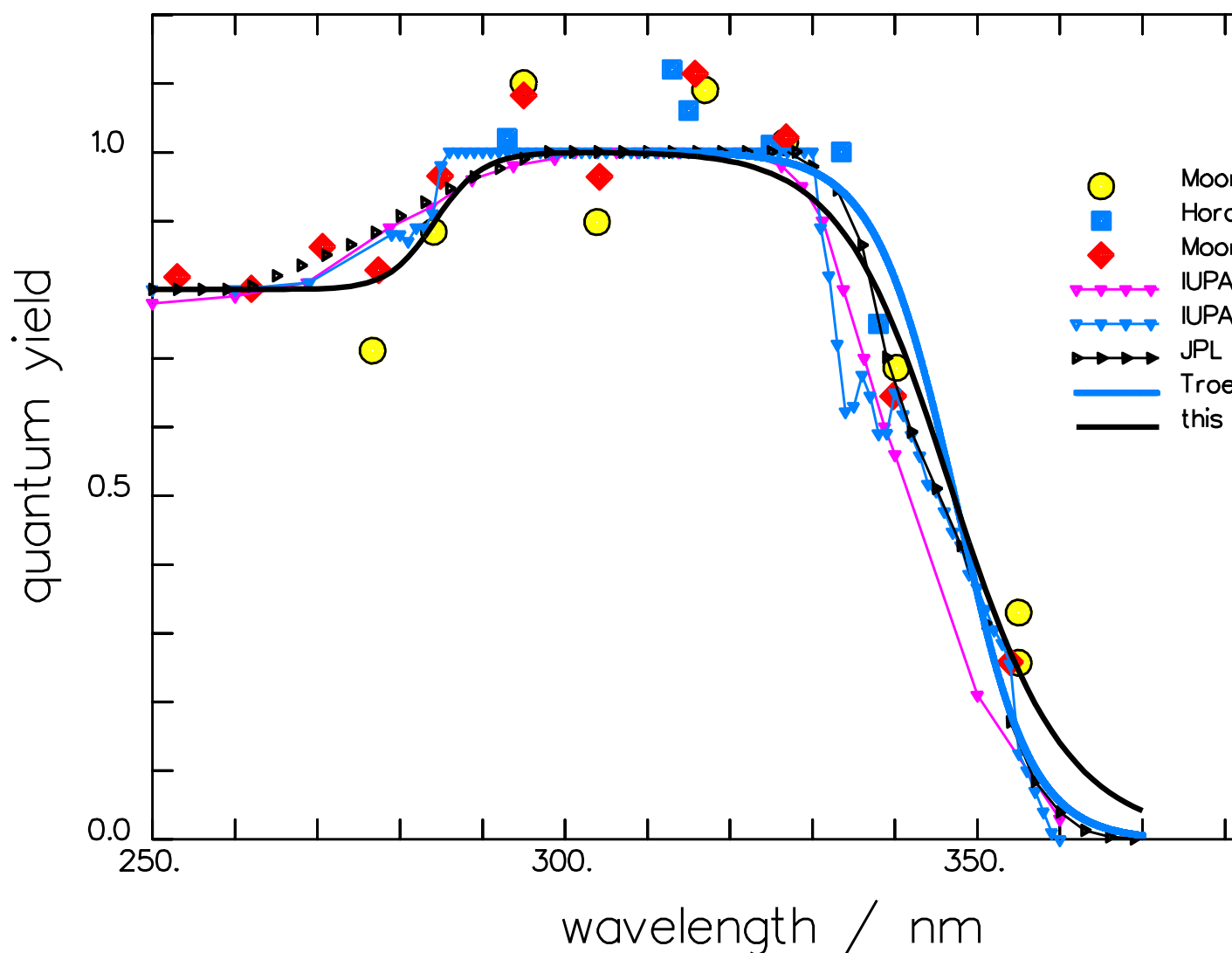
5

6

7



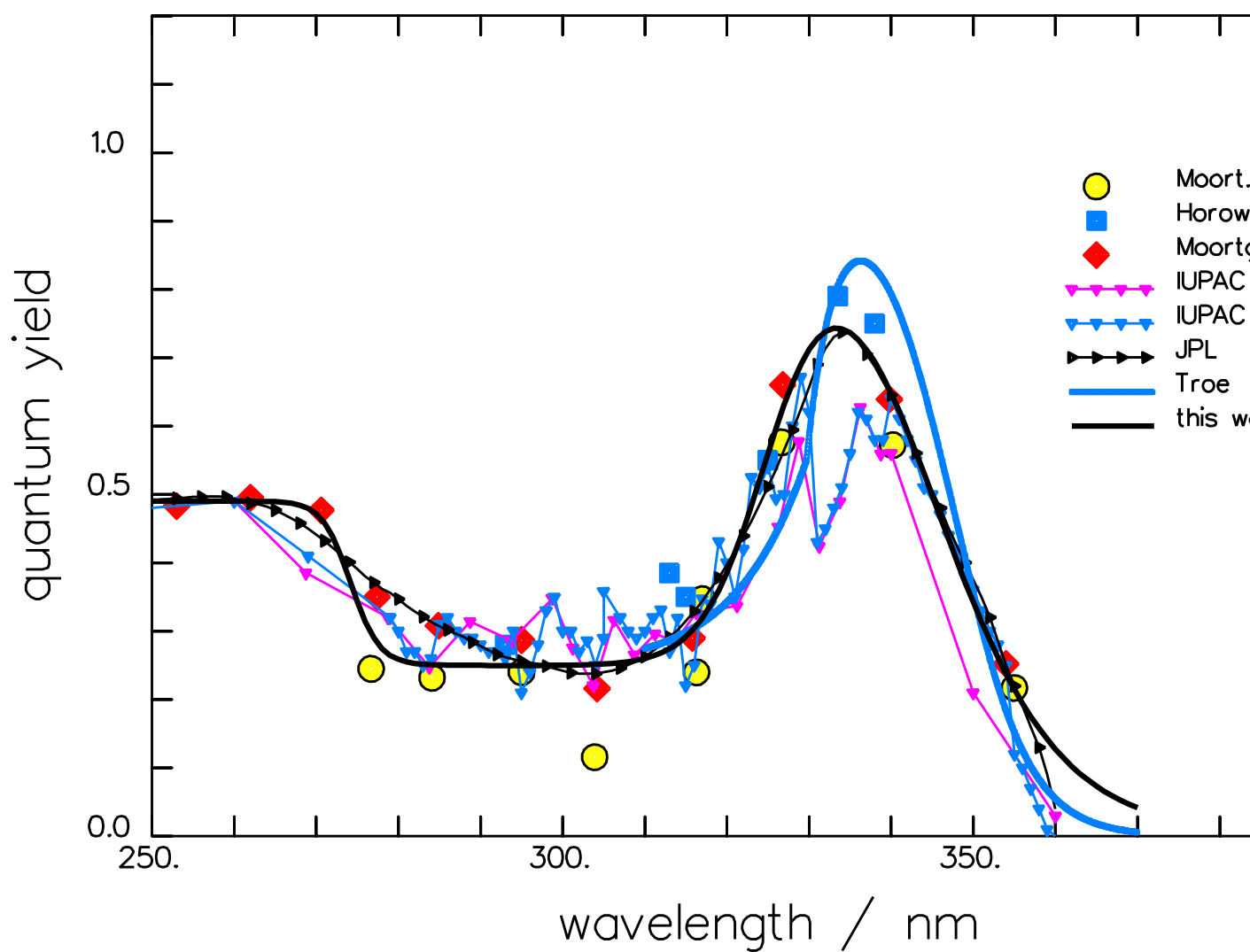
1  
2  
3  
4 **Figure 1:** Spectrum of the quantum yield of the radical channel of the  $\text{CH}_2\text{O}$  photolysis at  
5 room temperature. Measured data used for the fit are indicated by the large full symbols  
6 (**Horowitz** and Calvert, 1978; **Moortgat** et al., 1983; **Smith** et al., 2002; **Gorrotxategi**  
7 Carbajo et al., 2008). The present fit and the theoretical curve from **Troe** (2007) are given by  
8 full lines. Recommended data are represented by small symbols connected by a thin line: **JPL**  
9 (Sander et al., 2011); **IUPAC (2006)**, and **IUPAC (2013)**. The line structure observed by  
10 **Tatum Ernest** et al. (2012) is indicated by open circles and a dotted line.  
11



1  
2  
3  
4  
5  
6  
7  
8  
9  
10  
11

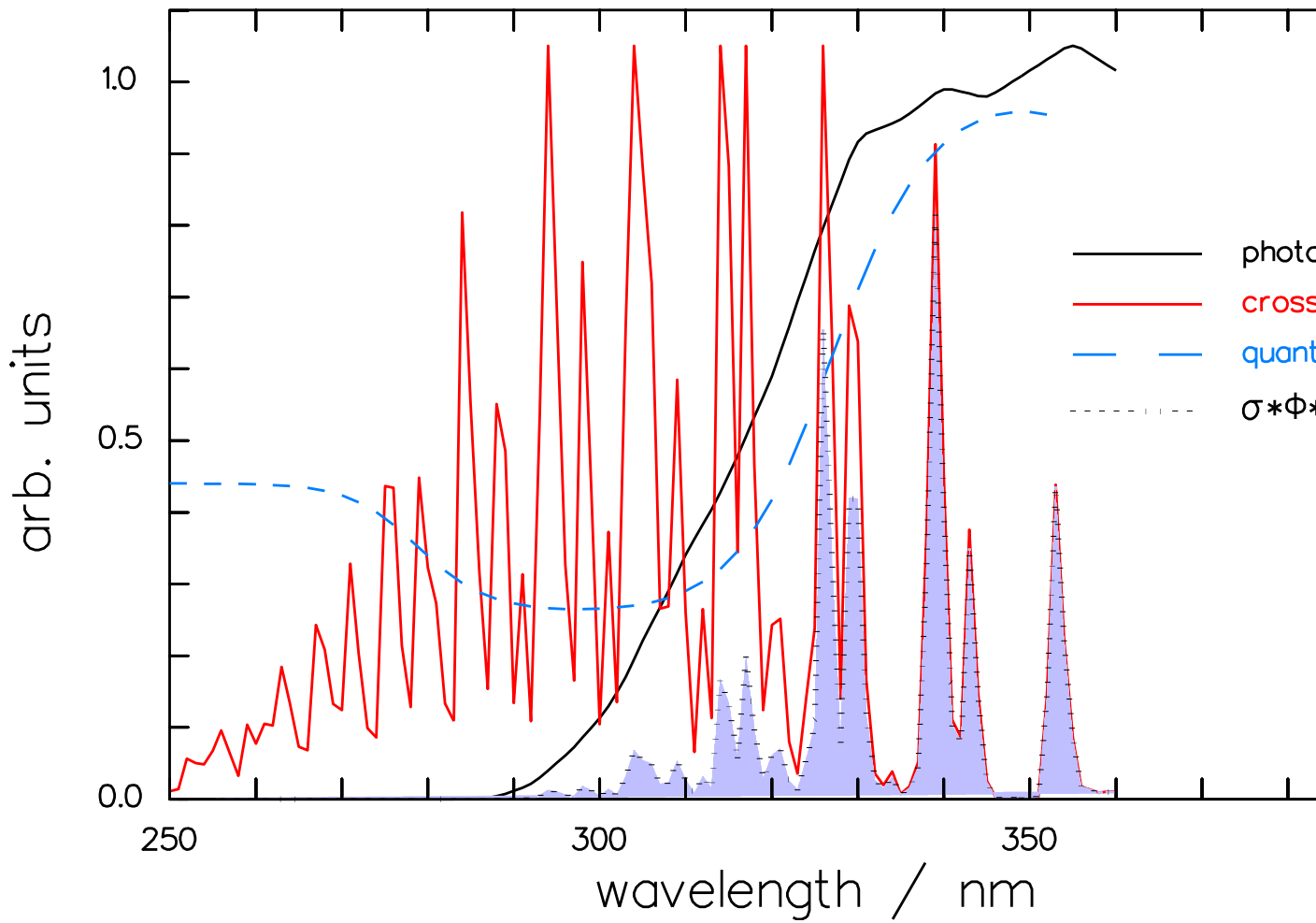
**Figure 2:** Spectrum of the quantum yield of the total CH<sub>2</sub>O photolysis at room temperature. Measured data used for the fit are indicated by the large full symbols (**Moort.79:** Moortgat and Warneck, 1979, **Horowitz** and Calvert, 1978; **Moortgat** et al., 1983). The present fit and the theoretical curve from **Troe** (2007) are given by full lines. Recommended data are represented by small symbols connected by a thin line: **JPL** (Sander et al., 2011); **IUPAC** (2006), and **IPUAC** (2013).





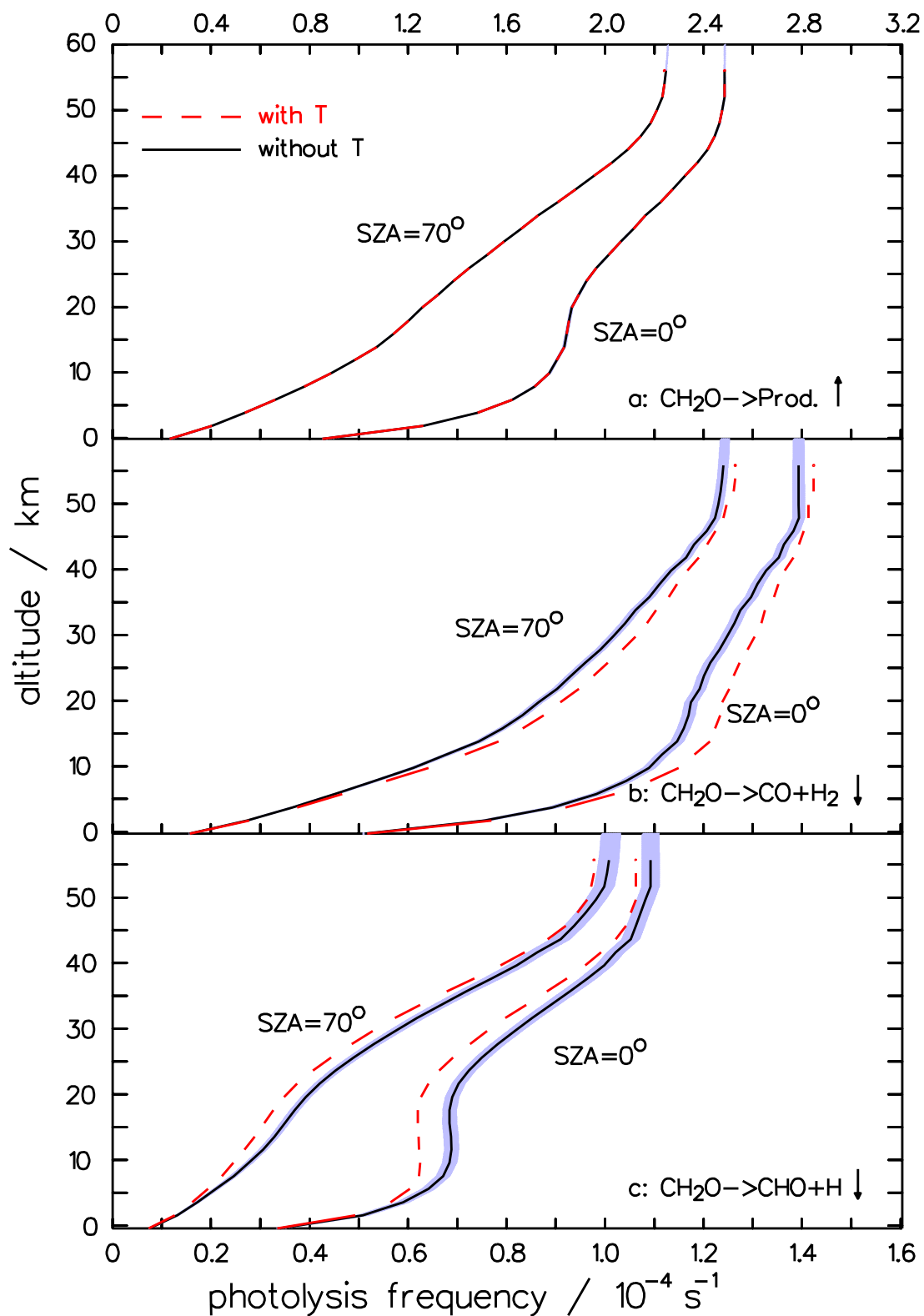
1  
2  
3  
4  
5  
6  
7  
8  
9  
10  
11

**Figure 3:** Spectrum of the quantum yield of the molecular branch of the  $\text{CH}_2\text{O}$  photolysis at room temperature. Measured data used for the fit are indicated by the large full symbols (**Moort.79**: Moortgat and Warneck, 1979, **Horowitz** and Calvert, 1978; **Moortgat et al.**, 1983). The present fit and the theoretical curve from **Troe** (2007) are given by full lines. Recommended data are represented by small symbols connected by a thin line: **JPL** (Sander et al., 2011); **IUPAC (2006)**, and **IUPAC (2013)**.

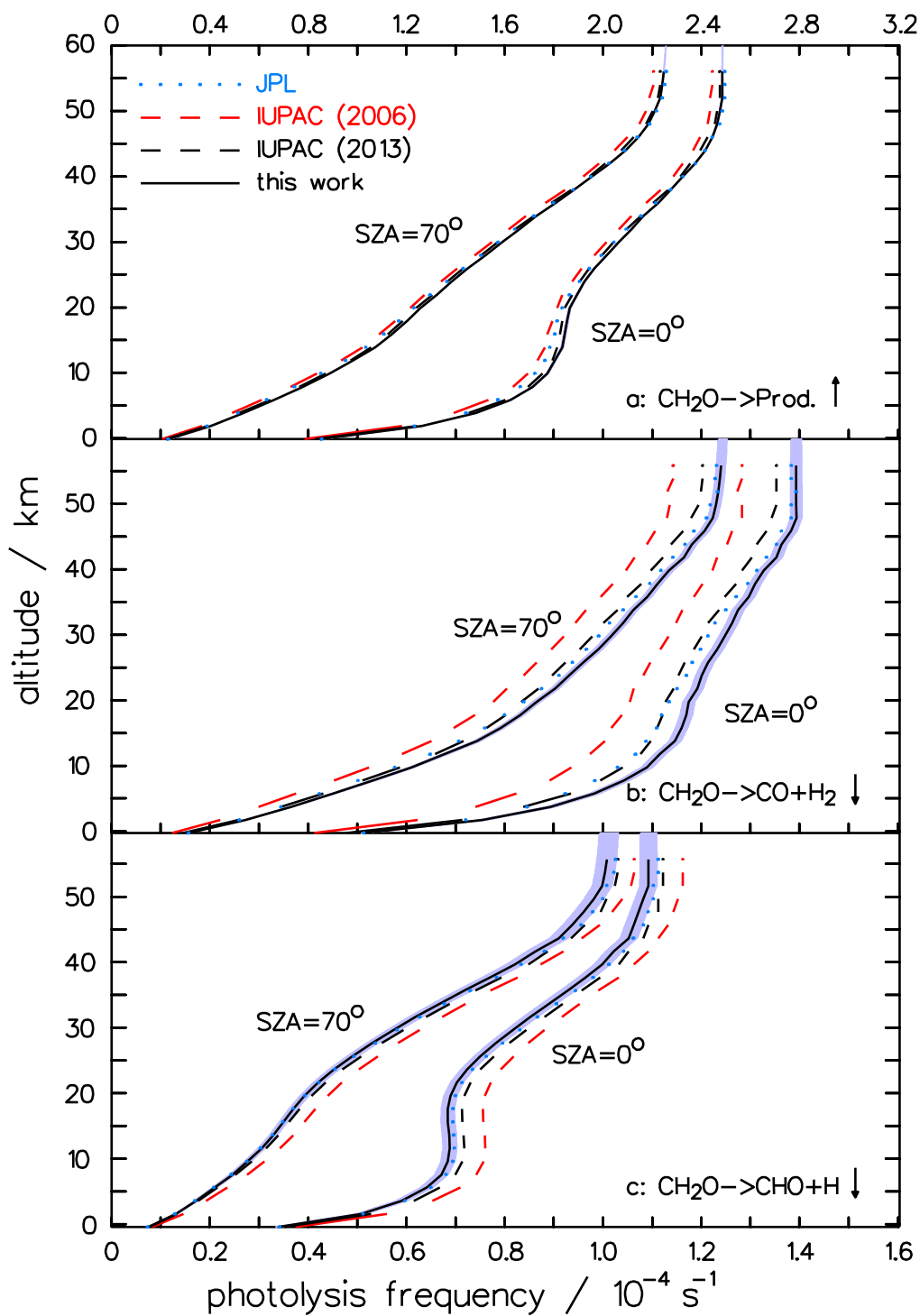


1  
2  
3  
4  
5  
6  
7  
8

**Figure 4:** Spectra of the actinic photon flux density (WMO, 1985), the optical absorption cross section (Gratien et al., 2007) and  $\Phi_{mol}$  at 30 km altitude,  $33^\circ$  solar zenith angle, 227 K. The shaded area represents the integrand  $\sigma \cdot \Phi \cdot F_\lambda$  of Eq.(11).



1  
 2 **Figure 5:** Impact of a temperature dependent quantum yield,  $\Phi_{\text{rad}}$ , on the altitudinal profile of  
 3 the photolysis of formaldehyde: total photolysis (a), molecular channel (b), and radical  
 4 channel (c). The dashed line indicates the impact of the temperature dependence of  $\Phi_{\text{rad}}$  given  
 5 by Troe (2007). The shaded areas mark the  $1\sigma$  error bounds of the profiles based on the errors  
 6 of the fitting parameters for the present quantum yields. The frequencies are depicted for two  
 7 solar zenith angles (SZA). (The arrows point to the related ordinate)



1  
 2  
 3 **Figure 6:** Comparison of the altitudinal profiles of the photolysis frequencies of  
 4 formaldehyde from **JPL** (Sander et al., 2011); **IUPAC (2006)**, **IUPAC (2013)**, and the  
 5 present work: total photolysis (a), molecular channel (b), and radical channel (c). The  
 6 frequencies are depicted for two solar zenith angles (SZA). The shaded areas mark the  $1\sigma$   
 7 error bounds of the profiles based on the errors of the fitting parameters for the present  
 8 quantum yields. (The arrows point to the related ordinate)